Convention Special Issue - 2019

J. Indian Chem. Soc.,
Vol. 96, October 2019, pp. 1317-1331

An azido adduct of Schiff base manganese(III) phenoxo-bridged dimer in dual action: Sensing of benzene and phenoxazinone synthase activity

Partha Pratim Chakrabarty[a,b], Pritam Singh[a], Kamalika Sen*[a], Sandip Saha*[b] and Dieter Schollmeyer[c]

[a]Department of Chemistry, University of Calcutta, 92, Acharya Prafulla Chandra Road, Kolkata-700 009, India

E-mail: kamalchem.roy@gmail.com

[b]Department of Chemistry, Acharya Prafulla Chandra College, New Barrackpur, Kolkata-700 131, India

E-mail: sandipsaha2000@yahoo.com

[c]Institut fur Organische Chemie, Universit at Mainz, Duesbergweg 10-14 55099 Mainz, Germany

Manuscript received online 16 September 2019, accepted 01 October 2019

A binuclear phenoxo-bridged azido adduct of manganese(III) Schiff base complex has been synthesized. Structure analysis reveals that two units of the tetradentate Schiff base forms the equatorial plane around manganese(III) center in this complex. One of the axial positions is occupied by a terminal azide, while the remaining axial position of the octahedron is connected to a phenoxo group of the neighboring monomeric unit which forms the bridge in the dimer. The benzene rings attached to the two adjacent Mn atoms through O are slightly opened up at their rear ends. The distance between the benzene rings facing each other gradually increase outward. This opens up the possibility of interaction with guest molecules which thereby results in sensing of the analyte molecules. The synthesized binuclear complex was evidently found to have dual actions in sensing and catalysis. Interesting spectral features of the compound allow it to act as a sensor towards an aromatic hydrocarbon, benzene down to ~0.06 mM (4.37 ppm) concentration range. A promising catalytic phenoxazinone synthase activity was also observed in the same compound due to the oxidation of *o*-aminophenol (OAPH). The Michaelis binding constant (K_M), maximum velocity (V_{max}) and turnover number (k_{cat}) were found to be $(1.09\pm0.3)\times10^{-2}$ *M*, 5.77×10^{-8} *M* s^{-1} and 20.77 h^{-1}, respectively. The rate determining step is governed by formation of substrate-catalyst adduct of OAPH with complex **1** followed by free radical mechanism. The structural and electronic parameters of complex **1** were justified by density functional theory (DFT) and time dependent density functional theory (TD-DFT) computations.

Keywords: Mn(III), Schiff base, sensor, benzene, phenoxazinone synthase activity, TD-DFT.

Introduction

The continuous evolution of metal assembled complexes of manganese have attracted considerable attention in recent years due to their various interesting properties like biomimetism, catalysis, molecular magnetism[1–3], etc. Manganese takes part in several essential life processes. On the other hand, polynuclear Mn(III) species are also found to play an important role in catalytic and biological fields especially as the oxygen evolving compound (OEC) of photosystem II (PS II)[4,5]. In this connection, Schiff base complexes of Mn^{3+} containing metal centers are of particular interest because the Mn^{3+} ion, whose oxidation state is stabilized in the N_2O_2 environment of tri/tetradentate Schiff bases. Accordingly, the self-assembly of the Mn(III) Schiff base with azide led to the formation of dinuclear entities[6–9] and frequently constrained one-dimensional (1D) chains[10–14].

Benzene is widely used as industrial solvents for synthesis of organic compounds. In spite of their well proven carcinogenic activities, such compounds are disposed relentlessly in the environment without proper pretreatment. Exposure of the living world to even minute quantities of such compounds is harmful and has long lasting effect. The American Conference of Governmental Industrial Hygienists (ACGIH) has restricted the occupational exposure limits for benzene as 0.5 ppm in air respectively, as threshold value-time weighted averages (TLV-TWA)[15]. Sensing of volatile organic compounds is therefore an upcoming research as is also evident from the recent literature reports[14,16–21].

Recently, low-cost and efficient nanoscale devices capable of fast and reversible detection of these compounds are being fabricated[14]. Ag nanoprism arrays coupled to aryl bridged polysilsesquioxane films are designed and fabricated through colloidal templating approach, which were found suitable to detect 30 ppm xylene or benzene in N_2 atmosphere[22]. Porous materials with tailored nanostructure cavities are yet another mode to trap and detect these volatile solvents with the aid of absorption and fluorescence spectrometry[16]. Apart from designing sensor materials, advanced technologies like non-dispersive infrared spectrophotometry, tunable diode laser spectroscopy, photoacoustic spectroscopy and high resolution localized surface plasmon resonance spectroscopy are also under investigation to detect these compounds at trace and ultra-trace quantities[20–22]. Some of the reported methods for detection of benzene along with the corresponding limit of detection (LOD) values are tabulated in Table 1.

Schiff base metal complexes are also coming up as potential sensor materials for several analytes[23]. The advantage with these complexes is that they have versatile spectral properties which are apt to show detectable changes if they react with analytes of special interest. When these compounds are dissolved in suitable solvents they exhibit characteristic spectral features which get modified upon interaction with certain analytes and hence can act as spectroscopic sensor materials. Recently we have reported two such cases where Schiff base metal complexes were found suitable for sensing application. In the first report selective sensing of perdisulfate and thiosulfate ions using Nd containing heterometallic Schiff base Cu complex[24]. In the second re-

Table 1. Comparison of previously reported sensing methods of benzene/xylene

Compound	Reagent(s)/Condition	Technique	LOD	Sample type	Interference	Ref.
Benzene	Polymer coated quartz crystal microbalance	Static headspace sampling technique	0.98 ppm	Gas	–	31
Benzene	Bioluminescent bacteria, at 37°C temperature	Optical detection	0.2% liquid volume	Gas	–	32
p-Xylene	$Cu(NO_3)_2 \cdot 3H_2O$ and trimesic acid	Gravimetric method	400 ppb	Vapor	Benzene, toluene and ethylbenzene	33
Benzene	$[Ru(5,6\text{-}Me_2Phen)_3](tfpb)_2$, heating at 100°C, followed by cooling to room temperature, then exposed to N_2-atm.	Fluorescence spectroscopy	7600 ppm	Vapor	–	34
Benzene	Pd/i-diamond interface	Measuring current (I) as a function of voltage (V)	–	Gas	–	35
Benzene and xylene	Polyacrylate resin, spin coater with 1500 rpm	Optical detection	<10 ppm	Gas	Other volatile organic compounds having higher concentration	36
Benzene	TiO_2/SnO_2 nanoparticles; air flow rate is 240 mL/min; 220°C temperature	Cataluminescence	6 ppm	Vapor	No interference	37
Benzene	WO3 layer, Pt micro-heater, Pt interdigitated electrodes, 300°C temperature	Mass spectrometry	0.2 ppm	Gas	–	38
Benzene and *p*-xylene	Dibenzoylmethanat *o*-boron difluoride	Fluorescence spectroscopy	~ 20 ppm and ~10 ppm for benzene and *p*-xylene respectively	Gas	–	39
Benzene	$C_{36}H_{36}Mn_2N_{10}O_4$	Absorption spectroscopy	4.37 ppm	Liquid	–	This work

port another Cu based Schiff base complex was found to sense an organophosphorous compound[25].

On the other hand a quick literature survey establishes a prominent growth in the catalytic activity of the transition metal Schiff base complexes, phenoxazinone synthase in particular in addition to their conventional catecholase like activity[26–29]. The essence of compounds having phenoxazinone synthase activity lies in their ability to catalyze the penultimate reaction step of the biosynthesis of actinomycin D, an antibiotic produced by *Streptomyces antibioticus*[30]. Two molecules of 3-hydroxy-4-methylanthranilic acid pentapeptide lactone undergo an oxidative condensation to form the phenoxazinone chromophore of actinomycin D which is also a potent destroyer of the viability of cancer cells. Herein, we report the synthesis and characterization of an azido adduct of Schiff base manganese(III) phenoxo-bridged dimer with its dual role in sensing activity towards benzene at ultra-trace levels along with a promising phenoxazinone synthase activity. To the best of our knowledge such dual action in a single transition metal Schiff base complex is reported here for the first time.

The single crystal X-ray diffraction analysis of complex **1** reveals that its structure has similar features with those of the one reported by Saha *et al.* in 2004[9]. In this case, the tridentate Schiff base ligand has undergone hydrolysis at benzylic position of N-benzyl ethylene diamine, resulting further condensation of -NH_2 group with that of another *o*-hydroxyacetophenone molecule. Therefore, the complex was produced involving tetradentate N_2O_2 donor Schiff base ligands instead of N_2O donor. In the previous report[9] the complex was thoroughly characterized by different spectroscopic tools and magnetic property of the complex was determined which showed antiferromagnetic character possessing an S = 4 ground state at room temperature. No further application based studies were reported therein. Therefore identical single crystal X-ray data in the present work prompted us to explore some interesting properties of the compound. The complex possesses a different CCDC number mainly due to difference in cell parameters. There are differences in cell parameters between previously reported complex and our complex mainly due to the difference in temperature of data collection. The ORTEP diagram of the complex **1** and crystallographic data for complex **1** have been given in the Fig. 1 and Table 2 (CCDC No. of **1** is 1557254).

Experimental

Materials and instrumentation

N-Benzyl ethylenediamine and *o*-hydroxyacetophenone were purchased from Sigma-Aldrich, manganese(II) acetate trihydrate, sodium azide, methanol and benzene were of AR grade and used as received. All other chemicals used were of analytical grade. IR spectra were recorded in KBr pellets within the range 4000–400 cm^{-1} on a Perkin-Elmer Spectrum 65 FTIR spectrometer. Elemental analyses were carried out using a Heraeus CHN-O-Rapid elemental analyzer.

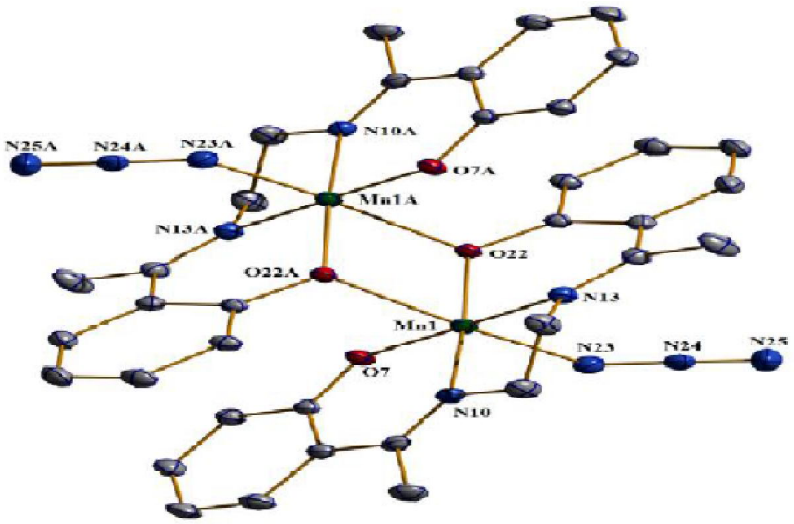

Fig. 1. Ortep view of complex **1**. Atoms are shown as 30% thermal ellipsoids. H atoms are omitted for clarity [Symmetry Code: A = -x, -y, -z].

Table 2. Crystallographic data for **1**

Crystal data	Complex **1**	Crystal data	Complex **1**
Empirical formula	$C_{36}H_{36}Mn_2N_{10}O_4$	Z	2
Formula weight	782.63	Temperature (K)	173(2)
Crystal dimension (mm)	0.26×0.23×0.09	D_{calc} (g cm^{-3})	1.545
Crystal system	Monoclinic	μ (mm^{-1})	0.809
Space group	'P 21/n'	$F(000)$	808
a (Å)	7.7658(2)	θ (°)	2.6–27.8
b (Å)	19.6118(6)	Total data	18707
c (Å)	11.0534(3)	Unique data	4019
α (°)	90.00	R	0.0301
β (°)	92.2110(8)	R_w	0.0799
γ (°)	90.00	Goodness-of-fit on F^2, S	1.042
V (Å^3)	1682.19(8)	R_{int}	0.0288

The UV-Visible spectra were obtained using an Agilent 8453 diode array spectrophotometer. Total independent data for complex **1** was collected on a Bruker Smart Apex II CCD Area Detector equipped with a graphite monochromator Mo-K_α radiation (λ = 0.71073 Å). Electron spray ionization mass (ESI-MS positive) spectra were recorded on a MICROMASS Q-TOF mass spectrometer. The electro analytical instrument, BASi Epsilon-EC for cyclic voltammetric experiment in CH_2Cl_2 solutions containing 0.2 *M* tetrabutylammonium hexafluorophosphate as supporting electrolyte was used. The BASi platinum working electrode, platinum auxiliary electrode, Ag/AgCl reference electrode were used for the measurements. The redox potential data are referenced vs. ferrocenium/ferrocene, Fc^+/Fc, couple. Redox properties of complex **1** (in DMF solution) were investigated by cyclic voltammetry (CV) with tetrabutylammonium perchlorate as the supporting electrolyte at a scan rate of 100 mV s^{-1}.

Synthesis of complex 1

Caution! Since the metal azide is potentially explosive, only small amount of the material should be prepared and it should be handled with care.

To a solution of *o*-hydroxyacetophenone (2 mM, 0.26 g) in 20 mL methanol, N-benzyl ethylene diamine (2 mM, 0.50 g) was added dropwise and the resulting mixture was heated under reflux for 4 h. A methanolic solution of manganese(II) acetate trihydrate (2 mM, 0.52 g) was then added and the mixture was refluxed for another 2 h to obtain a deep-brown solution. The aqueous solution of NaN_3 (4 mM, 0.26 g) dissolved in minimum volume of water was then added dropwise to the refluxed mixture. Then the resulting mixture was stirred for about another 2 h and then filtered. The brown solution was then kept at room temperature for 7 days. Dark brown colored block shaped crystals of the product (complex **1**) were obtained. Complex **1**: yield of 70% (based on the weight taken of manganese(II) acetate trihydrate). Anal. Calcd. for $C_{36}H_{36}Mn_2N_{10}O_4$: C, 43.5; H, 4.7; N, 19.9. Found: C, 44.0; H, 4.9; N, 19.1%.

Sensing application

0.1 mM solution of complex **1** was prepared in DMSO for absorption spectroscopic studies. Aliquots of benzene were added to this solution to get final concentration in the range 0.028–0.785 mM. The change in the spectral pattern was recorded with each successive addition.

Catalytic oxidation of o-aminophenol

Functional model for phenoxazinone synthase activity was examined by the reacting 1.0×10^{-5} *M* dioxygen-saturated methanolic solutions of the complex with 0.01 *M* solution of 2-aminophenol (OAPH) at 25°C. Upon formation of the phenoxazinone chromophore, there is a successive increase in absorbance band at *ca.* 433 nm which was monitored spectrophotometrically. To evaluate the rate dependence of the reaction on OAPH concentration and various kinetic parameters like V_{max}, K_M, K_{cat}, 1.0×10^{-5} *M* solution of the complexes were mixed with various concentration of substrate maintaining minimum 10-folds excess to that of catalyst to retain the pseudo-first order condition. Rate of a reaction was evaluated from the initial rate method, and the average initial rate over three independent measurements was recorded.

Theoretical calculations

Electronic structure analysis of complex **1** (in the gaseous phase) was carried out using the Gaussian09[40] program suite. Without symmetrical constrains, all geometries for ground states (S0) were optimized with gradient-corrected exchange functional B3LYP and 6-311+G** basis set[41,42]. All minimized geometries were confirmed by frequency calculations with true minima. One of the extensively used gradient corrected correlated functional is the LYP functional of Lee, Yang and Parr. In 1988 Becke proposed a famous gradient-corrected exchange functional. The combination of these two methods is the B-LYP method. B3LYP model is known to be the best of these hybrids functional where Becke's three-parameter formulation was used as hybrid model with corrections for both gradient and exchange correlations used for optimization of the complex **1**[41,42]. The coordinates of asymmetric unit of complex **1** obtained from single crystal X-ray diffraction data were used for computation using the LanL2DZ effective core potential (ECP) set of Hay and Wadt[43–45] for manganese atom and the standard 6-31+G(d) basis set for C, H, N and O atoms respectively[46,47]. To confirm local minima, only positive eigen values of optimized geometries, the vibrational frequency calculations were carried out. Time-dependent density functional theory (TD-DFT) was computed[48–50] in dimethylsulfoxide (DMSO) (ε = 46.826) using conductor-like polarizable continuum model (CPCM)[51–53] with the same B3LYP level basis set to verify the solvent effect. The excited states of the complex were calculated by time dependent density functional theory (TD-DFT) method with the same basis set. GAUSSSUM 3.0[54] was used to calculate the percentage contributions of ligand, co-ligand and metal ion to each molecular orbital.

Hirshfeld surface analysis

Hirshfeld surface analysis have been done using Crystal Explorer version 17.5[55]. The normalized contact distance (d_{norm}) based on d_i and d_e has been determined by the given equation where r^{vdW} is the van der Waals (vdW) radius of the appropriate atom internal or external to the surface.

$$d_{norm} = \frac{(d_i - r_i^{vdW})}{r_i^{vdW}} + \frac{(d_e - r_e^{vdW})}{r_e^{vdW}}$$

d_{norm} becomes negative for shorter contacts than vdW separations and becomes positive for contacts greater than vdW separations, and is displayed using a red-white-blue color scheme, where red highlights shorter contacts, white is used for contacts around the vdW separation, and blue is for longer contacts[56].

Results and discussion

Synthesis

The ligand was prepared by the 1:1 condensation of N-benzyl ethylene diamine with *o*-hydroxyacetophenone in methanol. The methanolic solution of the ligand was added to a methanolic solution of manganese(II) acetate trihydrate and this complex reacts with sodium azide in methanol-water mixture in refluxing condition to prepare the dinuclear complex **1**. Such complexes are generally obtained both from manganese(II) acetate trihydrate and manganese(III) acetate dihydrate. When manganese(II) acetate trihydrate is used it undergoes aerial oxidation during the course of the reaction in presence of this kind of tetradentate Schiff bases[6–13]. Complex **1** was characterized by IR spectroscopy and CHN analysis.

Cyclic voltammetry

The cyclic voltammogram of the complex **1** (Fig. 2) shows a cathodic peak at potential –0.309 mV indicating the reduction of Mn(III) to Mn(II). The anodic peak appears at –0.210 mV for oxidation of Mn(II) to Mn(III) indicating a quasi-reversible process. This result indicates that complex **1** is capable to exhibit redox acitivity.

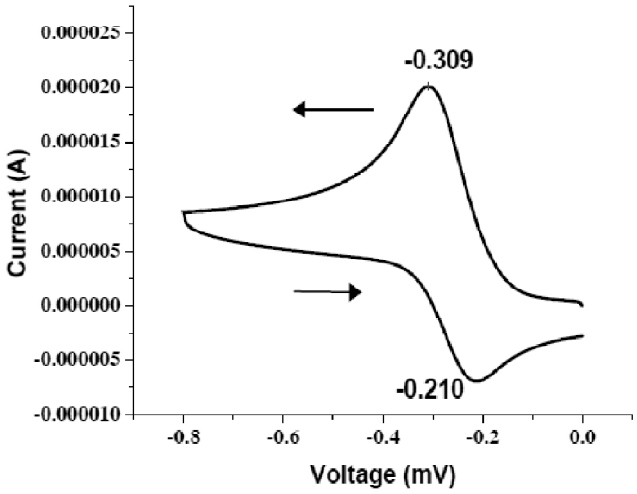

Fig. 2. Cyclic voltammogram of complex **1** against Ag/AgCl reference electrode.

Sensing application

The comparative absorption spectra of the Schiff base ligand with that of the complex **1** in DMSO solution is shown in Fig. 3. The characteristic λ_{max} for the complex **1** appears at a wavelength of 258 nm which is due to the aromatic moiety of the benzene ring present in the complex[57]. The Schiff base ligand shows an additional peak at 320 nm due to a $\pi \rightarrow \pi^*$ transition arising out of the azomethine group. Further, it is also observable from the low molar extinction coefficient (ε) value of 196 L mol^{-1} cm^{-1} calculated using the absorption spectrum with increasing concentrations of complex **1** at this λ_{max} which arises for $n \rightarrow \pi^*$ transition in the molecule (Fig. 4). With addition of increasing concentrations (0.028–0.785 mM) of benzene to this system, a prominent increase in the absorption intensity is observed. This arises due to the attractive polarization forces between the π electron densities of the added benzene with that of the complex molecule itself. The absorption intensity increases with increasing benzene concentrations due to increased π electron density in the system (Fig. 5). The possibility of such spectral changes is nullified both in the ligand solution as well as in blank DMSO medium (negligible change in spectra, figure not shown). Different analytical parameters for the spectral detection of benzene using complex **1** are tabulated in Table 3. The possibility of similar kind of detection for different other organic solvents like toluene and quinoline were also explored and were not found to yield interesting results using complex **1**.

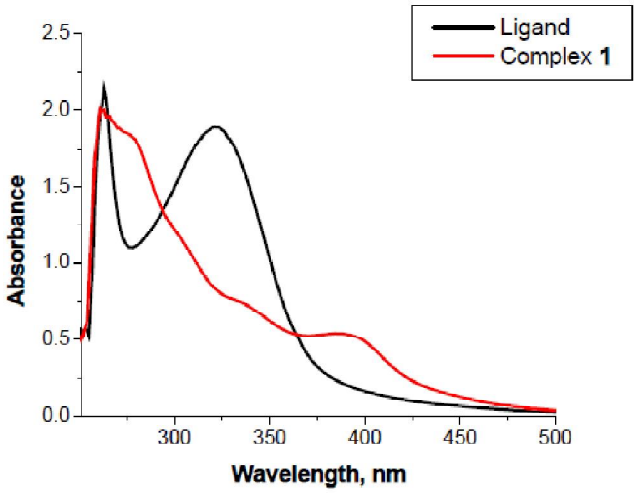

Fig. 3. Absorption spectra of 0.1 mM solutions each of the Schiff base ligand and complex.

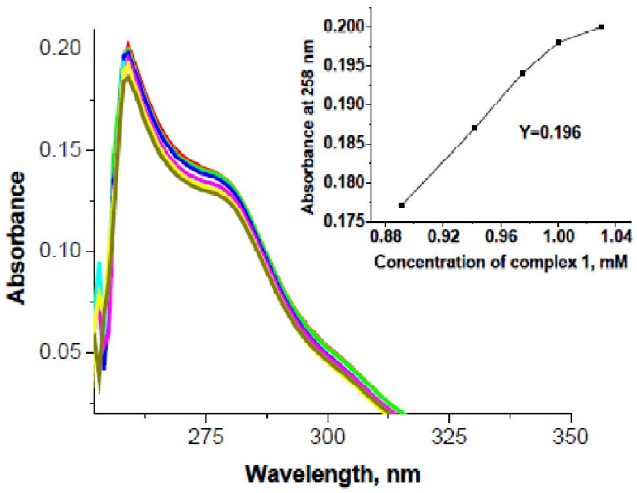

Fig. 4. Absorption spectral profile of complex **1** with increasing concentrations.

Table 3. Different analytical parameters for the detection of benzene

Parameter	Detection of benzene
Regression equation	$Y = sX$
Slope (s) (mmol^{-1})	0.96
Correlation coefficient (R^2)	0.87
Standard deviation (σ)	0.016
Limit of detection (LOD = 3.3×σ/s (mM))	0.06
Limit of quantification (LOQ = 10×σ/s (mM))	0.17
Linear range (mM)	0.028 to 0.166
λ_{max} (nm)	228

The results are also suggested by IR spectral data shown in Fig. 6

Phenoxazinone synthase like activity

Catalytic oxidation of *o*-aminophenol (OAPH) was spectrophotometrically studied in dioxygen-saturated methanol solution at 25°C. It is essential to validate the efficiency of a complex for deploying it as a catalyst for the oxidation of *o*-aminophenol to 2-aminophenoxazine-3-one. Initially, 1×10^{-5} *M* solution of the complex **1** was reacted with a 0.01 *M* solution of 2-aminophenol under aerobic conditions. Upon continual catalytic oxidation of 2-aminophenol (OAPH), the characteristic absorption band *ca*. at 433 nm was obtained which gradually increases by time endorsing the catalytic activity of the complex resulted from oxidation of OAPH to 2-aminophenoxazine-3-one under aerobic condition. The enhancement of absorbance band at *ca*. 433 nm has been stud-

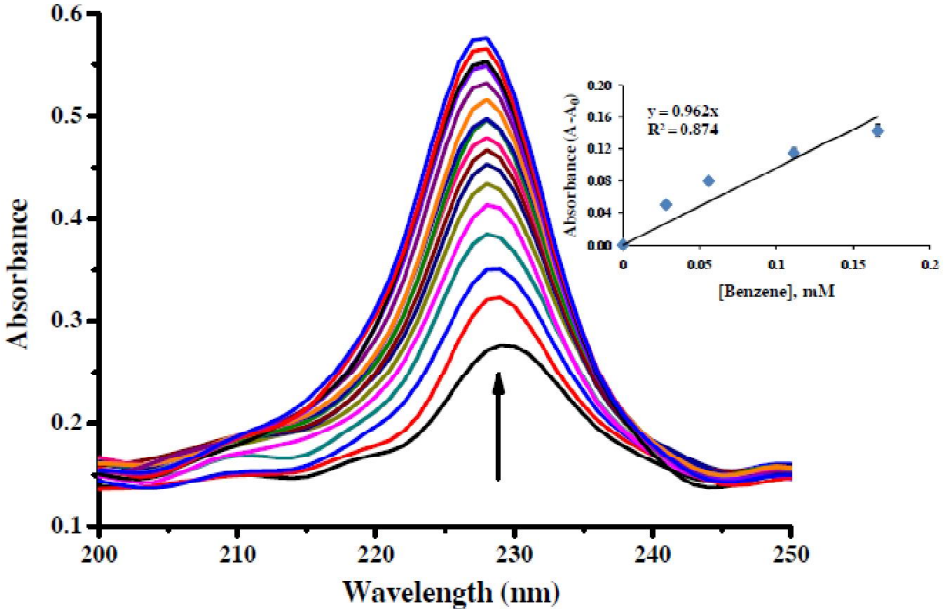

Fig. 5. Absorption spectral profile of 0.1 mM solution of complex **1** with increasing addition of benzene in 0.01 mL portions, in the concentration range 0.028–0.785 mM. The linear range is found between 0.028–0.166 mM.

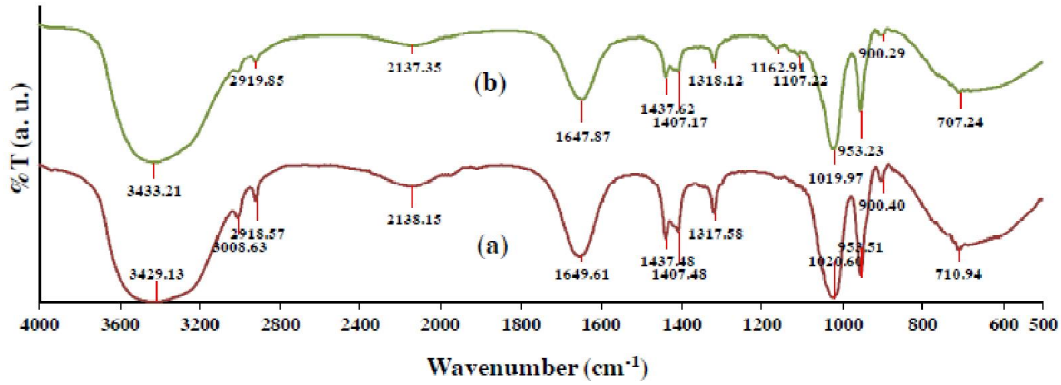

Fig. 6. IR spectra of (a) pure complex **1** and (b) complex **1** treated with benzene.

ied by absorption spectroscopy for a period of 2 h after. The time-resolved spectral profile of complex **1** is shown in Fig. 7. Under identical conditions a blank experiment in absence of the complex **1** has been carried out, which does not result any substantial enhancement of absorption intensity *ca*. at 433 nm. It implies that complex **1** is solely responsible for catalyzing oxidation process of *o*-aminophenol to 2-aminophenoxazine-3-one under aerobic condition. In order to understand the degree of catalytic efficiency of complex **1**, a detail kinetic study was performed at 25°C. For this purpose, 1×10^{-5} *M* solution of the complex **1** was reacted with at least 10-fold excess concentration of substrate solution to maintain the pseudo-first order reaction condition. In each case a particular OAPH ratio to that of the complex has been maintained and time scan at the maximum band i.e. 433 nm was monitored for a period of 1 h. Each experiment was performed thrice and average values were noted. From each kinetic measurement a straight line has been obtained where absorbance was plotted against time. The initial rate was determined by linear regression from the slope of the absorbance versus time. The initial rate of the reactions versus concentrations of the substrate plot shows rate saturation

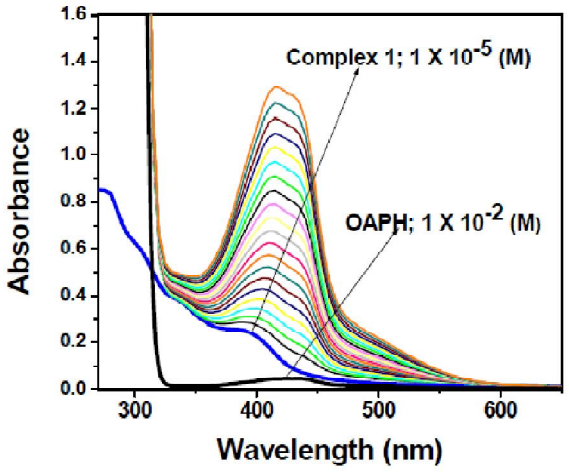

Fig. 7. UV-Vis spectral scans (1 cm path length) showing the increase in phenoxazinone chromophore band at 433 nm after the addition of *o*-aminophenol (10^{-2} *M*) to a solution of complex **1** (1×10^{-5} *M*) in methanol at 25°C. The spectra were recorded for the period of 2 h.

kinetics as depicted in Fig. 8. In the catalytic cycle, a substrate-catalyst adduct of OAPH is formed with complex **1** followed by release of the oxidized product of OAPH in irreversible manner which is the rate determining step (r.d.s.). The successive steps are governed by an electron transfer process and a free radical mechanism thereafter (Scheme 1). The free azide generated from complex **1** during the adduct formation converts the OAPH to its free radical. The free radical then immediately gets oxidized to benzoquinone monoimine (BQMI) which further undergoes oxidative dimerisation to generate phenoxazinone. Since the kinetic measurements were performed in such a manner that it retains pseudo-first order reaction condition that it can be fitted to Michaelis-Menten model. The parameters namely V_{max}, K_M, and k_{cat} can be evaluated from Lineweaver-Burk plot which was obtained by linearizing Michaelis-Menten equation. The observed and simulated initial rate versus substrate concentration plot and the Lineweaver-Burk plot for the complex was shown in Fig. 9. Michaelis binding constant (K_M) and V_{max} were calculated to be $(1.09\pm0.3)\times10^{-2}$ *M* and 5.77×10^{-8} *M* s^{-1}, respectively. The turnover number (k_{cat}) value is calculated by dividing the V_{max} with the concentration of the complex used, and is found to be 20.77 h^{-1}.

ESI mass study

Catalytic behaviour of complex **1** encourages us to perform mass spectrometry of the reaction mixture (complex **1** + OAPH) to have information regarding the important intermediates. Complex **1** was mixed with around 50-folds excess of OAPH and the mixture was used for spectral study. A peak at *m/z* 953.18 was arrested which corresponds to the complex-substrate adduct of formula $[Mn_2L_2(OAPH)_2 + K]^+$. The peak at *m/z* 953.18 implies that the azido co-ligands are

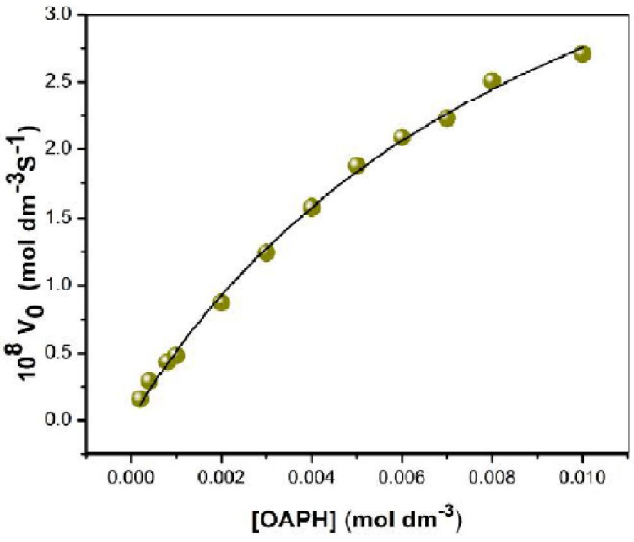

Fig. 8. Initial rate verses substrate concentration plot for the oxidation of 2-aminophenol catalyzed by complex **1** in dioxygen-saturated methanol at 25°C. Symbols and solid line represents the experimental and simulated profiles, respectively.

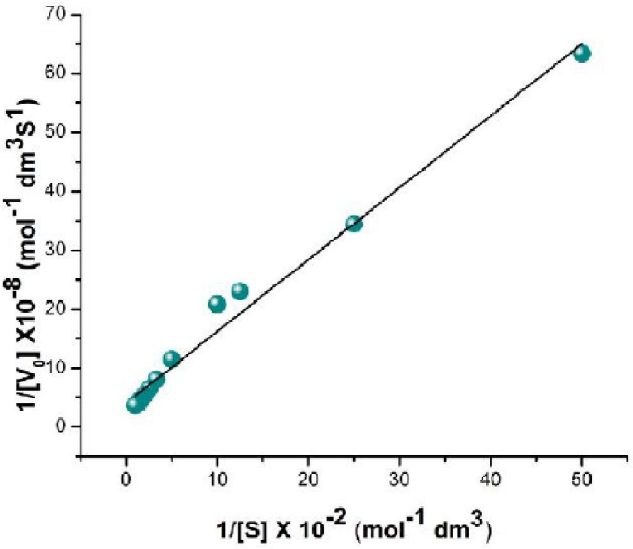

Fig. 9. Lineweaver-Burk plots for the oxidation of *o*-aminophenol catalyzed by complex **1** in aerobic condition. Symbols and solid line represents the experimental and simulated profiles, respectively.

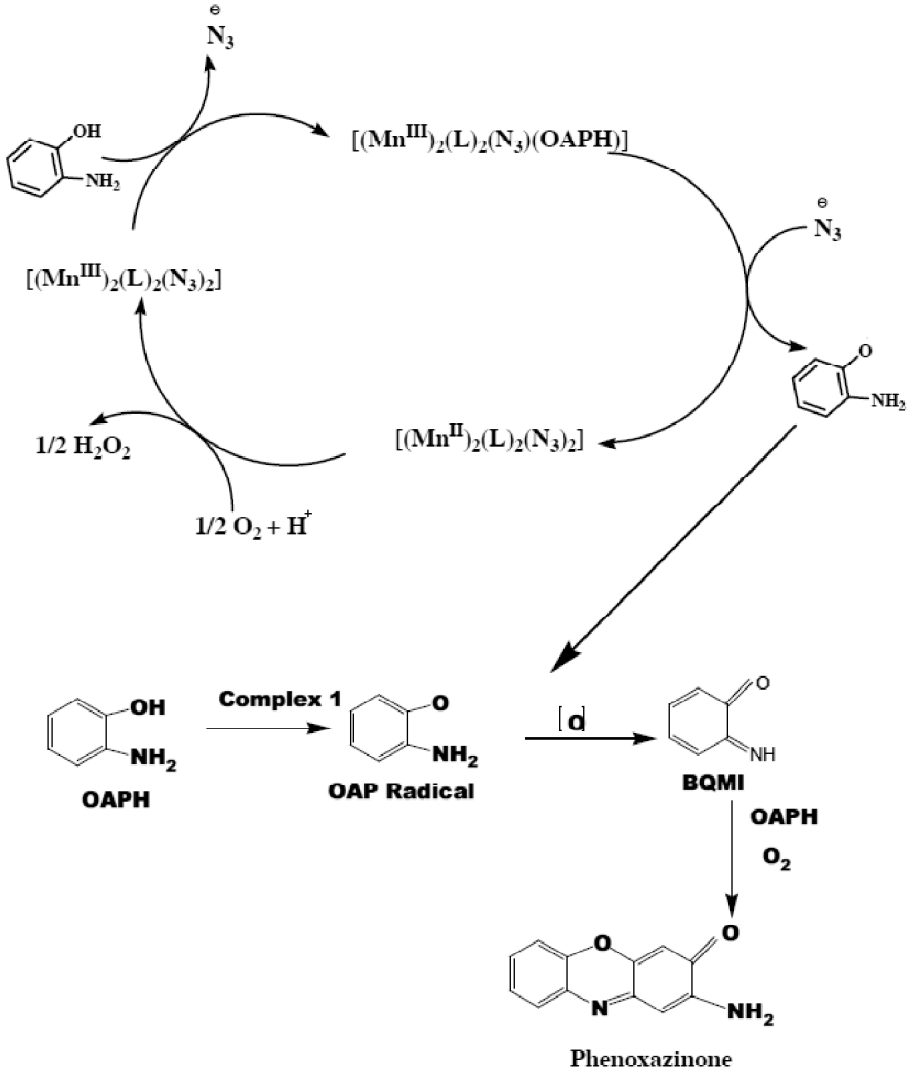

Scheme 1. Probable mechanistic pathway for the formation of the phenoxazinone chromophore.

loosely bound and they detach when OAPH gets attached to the Mn(III) centre. Two interesting peaks were found at *m/z* 212.9947 and 215.0113 correspond to 2-amino-3*H*-phenoxazin-3-one and 2-amino-10*H*-phenoxazin-3-ol, respectively (Fig. 10). So, it is proposed that at r.d.s. two molecules of OAP get attached to the complex by replacing loosely bound azido ions and results formation of OAP radical. Therefore, the complex itself gets reduced to Mn(II) system. Then OAP radical could be transformed into *o*-benzoquinone monoimine (BQMI) in various ways including self-disproportionation. BQMI further reacts with dioxygen and OAPH to result phenoxazinone chromophore (Scheme 1).

Theoretical calculations

DFT study:

DFT/B3LYP method was used for optimization with the coordinates derived from single crystal X-ray diffraction data of complex **1**. Optimization for computational simplicity needs the asymmetric framework of complex **1**. Calculated bond distances and angles are comparable with that of X-ray data (Table 4). Mulliken charge distribution shows a positive charge of 0.823882 eV on metal atom. Table 5 contains the Mulliken charge distribution of complex **1**. Energy (eV) of some selected molecular orbitals of complex **1** is encapsulated in Table 6. Key electronic transitions and composition of M.O.s

Table 4. Bond angles (°) and bond distance (Å) for complex **1**

Bond distance (Å) and Bond angles(°) for complex **1**

	X-ray	Calcd.		X-ray	Calcd.
Mn1-O7	1.856(1)	1.9675	O7-Mn1-N10	90.64(5)	92.76
Mn1-N10	2.008(1)	2.1473	O7-Mn1-O22	95.29(5)	97.22
Mn1-N13	1.987(1)	2.0939	O7-Mn1-N23	92.91(5)	94.31
Mn1-O22	1.913(1)	2.0843	O7-Mn1-O22	85.65(4)	87.28
Mn1-N23	2.180(2)	2.2637	N10-Mn1-N13	84.58(6)	87.20
Mn1-O22	2.396(1)	2.4178	N10-Mn1-O22	168.22(5)	170.38
O22-Mn1	2.396(1)	2.4367	N10-Mn1-N23	95.04(6)	97.37
N23-N24	1.190(2)	1.2831	N10-Mn1-O22	91.77(5)	92.78
N24-N25	1.148(3)	1.2290	N13-Mn1-O22	88.59(5)	90.01
Mn1-O7	1.856(1)	2.0313	N13-Mn1-N23	92.32(6)	93.05
Mn1-N10	2.008(1)	2.1083	O22-Mn1-N23	94.81(5)	95.08
Mn1-N13	1.987(1)	2.2010	O22-Mn1-O22	78.58(4)	80.12
Mn1-N23	2.180(2)	2.2870	N23-Mn1-O22	173.05(5)	175.03
N10-C11	1.479(2)	1.6032	Mn1-O7-C2	130.7(1)	132.20
N23-N24	1.190(2)	1.2011	C1-C8-N10	121.6(1)	123.49
N24-N25	1.148(3)	1.2022	Mn1-N10-C8	128.9(1)	130.03
C2-O7	1.319(2)	1.4022	Mn1-N10-C11	110.8(1)	112.02
C8-N10	1.301(2)	1.4089	C8-N10-C11	120.0(1)	122..21
N10-C11	1.479(2)	1.6023	C12-N13-C14	123.8(1)	124.88
C12-N13	1.474(2)	1.5089	Mn1-O22-C20	122.06(9)	125.02
N13-C14	1.295(2)	1.3038	Mn1-O22-Mn1	101.42(5)	102.29
C20-O22-Mn1	115.91(9)	117.02	O22-Mn1-N13	89.67(5)	91.03
Mn1-N23-N24	124.4(1)	125.87	O22-Mn1-O22	78.58(4)	19.83
N23-N24-N25	178.6(2)	179.39	O22-Mn1-N23	173.05(5)	175.02
O22-Mn1-O7	85.65(4)	87.83	O7-Mn1-N10	90.64(5)	92.31
O22-Mn1-N10	91.77(5)	92.01	O7-Mn1-N13	173.21(5)	175.43
O7-Mn1-N13	173.21(5)	175.02	O7-Mn1-O22	95.29(5)	97.05
O7-Mn1-O22	95.29(5)	96.72	O7-Mn1-N23	92.91(5)	93.02
N10-Mn1-N23	95.04(6)	96.29	N10-Mn1-N13	84.58(6)	87.02
N13-Mn1-O22	88.59(5)	90.10	N10-Mn1-O22	168.22(5)	170.31
N13-Mn1-N23	92.32(6)	94.07	O22-Mn1-N23	94.81(5)	96.21
C8-N10-C11	120.0(1)	122.04	Mn1-O7-C2	130.7(1)	132.01
Mn1-O22-Mn1	101.42(5)	112.03	Mn1-N10-C8	128.9(1)	129.02
Mn1-O22-C20	115.91(9)	116.97	Mn1-N10-C11	110.8(1)	112.18
Mn1-O22-C20	122.06(9)	123.69	N23-N24-N25	178.6(2)	180.04
Mn1-N23-N24	124.4(1)	126.03			

of some selected ones are presented in Table 7. Contour plots of some selected M.O.s are given in Figs. 11 and 12. The energies of HOMO and LUMO are –5.4 eV (α-spin), –5.36 eV (β-spin) and –2.28 eV (α-spin), –1.73 eV (β-spin) respectively.

DFT study shows that molecular orbitals HOMO-5 to LUMO+5 (for α-spin and β-spin) have significant contribution from ligand as these orbitals are π-rich in character except HOMO-3, HOMO-1 and LUMO. LUMO+4 (α-spin) enjoy equal contribution from both metal and ligand. LUMO+4 to LUMO+2 (β-spin) and HOMO (β-spin) have major contri-

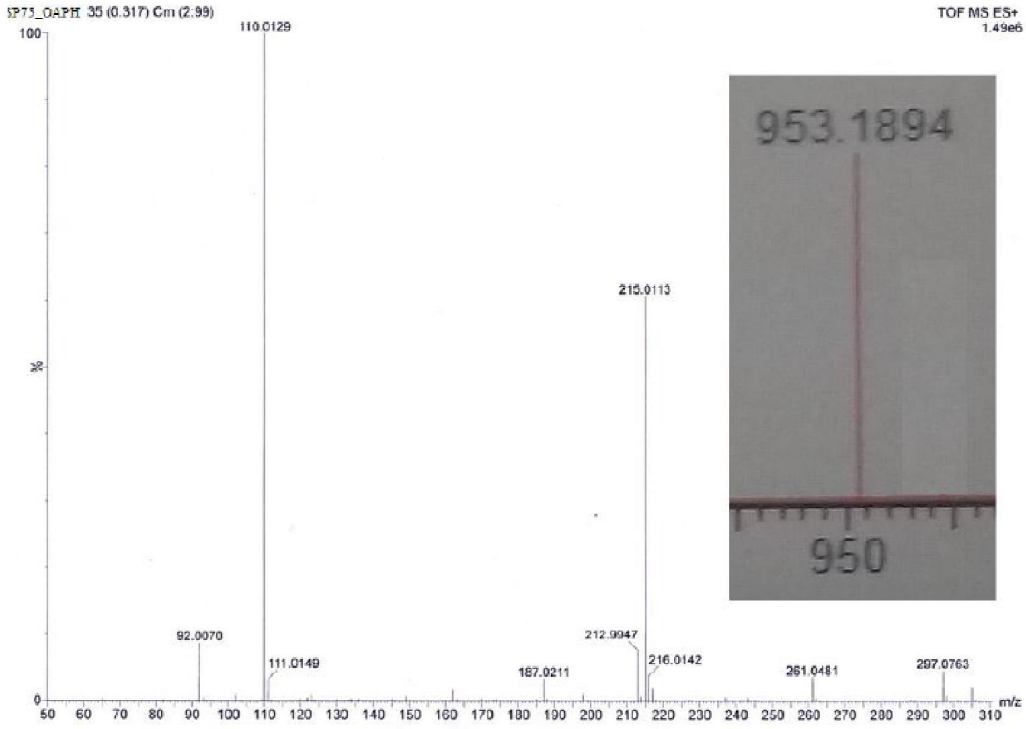

Fig. 10. ESI mass spectrum of complex **1** in presence of excess amount of OAPH.

Table 5. Mulliken atomic charge distribution of complex **1**

Complex **1**					
1	Mn	0.823882	25	N	–0.516080
2	C	0.057118	26	C	0.284381
3	C	0.398261	27	C	0.045352
4	C	–0.026918	28	C	–0.059423
6	C	0.025232	30	C	–0.004215
8	C	–0.008552	32	C	0.027249
10	C	–0.081298	34	C	–0.029748
12	O	–0.619581	36	C	0.402157
13	C	0.279984	37	C	0.071483
14	C	0.061889	41	O	–0.627278
18	N	–0.535018	42	N	–0.454092
19	C	0.222366	43	N	0.403449
22	C	0.208689	44	N	–0.349290

Sum of Mulliken charges with hydrogens summed into heavy atoms = 0.00000

Table 6. Energy (eV) and composition (%) of selected M.O.s of complex **1**

M.O.s (α-spin)	Energy (eV)	% Metal	% Ligand	% Azide (N_3)
LUMO+5	0.46	14	86	0
LUMO+4	0.39	10	89	1
LUMO+3	–0.6	57	43	0
LUMO+2	–1.58	2	98	0
LUMO+1	–1.67	7	92	1
LUMO	–2.28	57	17	26
HOMO	–5.4	10	82	8
HOMO-1	–5.79	5	19	76
HOMO-2	–5.9	4	86	10
HOMO-3	–6.26	43	27	30
HOMO-4	–6.65	25	63	12
HOMO-5	–6.7	15	65	20

Table-6 (contd.)

M.O.s (β-spin)	Energy (eV)	% Metal	% Ligand	% Azide (N_3)
LUMO+5	0.2	1	37	62
LUMO+4	–1.02	11	70	19
LUMO+3	–1.31	8	59	33
LUMO+2	–1.35	8	56	36
LUMO+1	–1.68	2	14	84
LUMO	–1.73	2	35	63
HOMO	–5.36	9	74	17
HOMO-1	–5.59	24	2	74
HOMO-2	–5.85	4	4	92
HOMO-3	–6.27	63	9	28
HOMO-4	–6.61	62	8	30
HOMO-5	–6.79	2	1	97

Table 7. Electronic transition calculated by TDDFT using B3LYP/CPCM method in DMSO solvent of complex **1**

Complex- **1**

$E_{excitation}$ (ev)	$\lambda_{excitation}$ (nm)	Osc. strength (*f*)	Key transition	Character
3.25	275.34	0.029	HOMO-2(α) → LUMO+4(α) (57%) HOMO(β) → LUMO+2(β) (23%)	π(L) → π*(L)
2.12	400.34	0.0039	HOMO(α) → LUMO(α) (58%) HOMO(β) → LUMO(β) (11%)	π(L) → π*(L)
2.61	412.69	0.0012	HOMO-1(α) → LUMO(α) (49%) HOMO-1(β) → LUMO+1(β) (27%)	π(L)/N_3^-(pπ) → π*(L)
2.65	420.25	0.0016	HOMO(α) → LUMO+1 (α) (37%) HOMO-2(β) → LUMO+1(β) (18%)	π(L)/N_3^-(pπ) → π*(L)

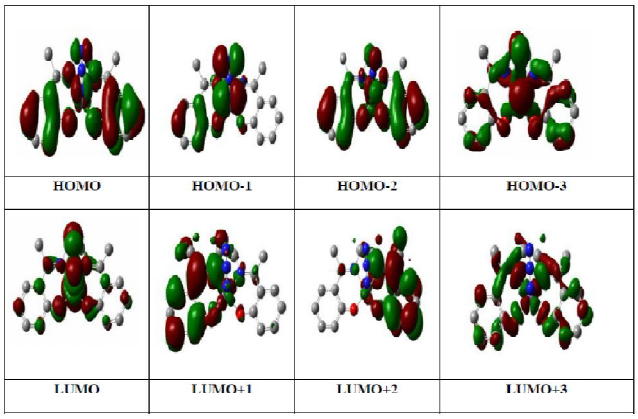

Fig. 11. Selected contour plots of α-spin molecular orbitals of complex **1.**

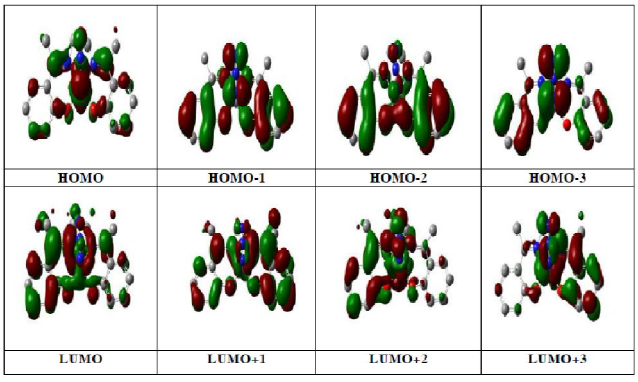

Fig. 12. Selected contour plots of β-spin molecular orbitals of complex **1**.

bution from ligand site. But, HOMO-1, HOMO-2 and HOMO-5 have major contributions from co-ligand i.e. azide side. HOMO-3 and HOMO-4 have major contribution from metal centre.

TD-DFT study:

TD-DFT calculations were performed using B3LYP/CPCM method using same basis sets in DMSO solvent to support the electronic transitions of complex **1**. Table 7 represents the calculated electronic transitions along with the calculated Oscillator Strength (*f*) of **1**. Complex **1** shows ligand based n-π and π-π* transitions around 258 nm and 390 nm, respectively. The bands at 258 nm and 390 nm can be theoretically correlated as the following excitations at 3.25 eV (λ = 275.34 nm, *f* = 0.0029), 2.12 eV (λ = 400.34 nm, *f* = 0.0039), 2.61 eV (λ = 412.69 nm, *f* = 0.0012) and 2.65 eV (λ = 420.25 nm, *f* = 0.0016), respectively and the assigned absorption bands are due to the contribution of HOMO-2(α) → LUMO+4(α) (57%), HOMO-2(β) → LUMO+1(β) (18%), HOMO(β) → LUMO+2(β) (23%), HOMO(α) → LUMO (α) (58%), HOMO(β) → LUMO(β) (11%), HOMO-1(α) → LUMO (α) (49%), HOMO-1(β) → LUMO+1(β) (27%) and HOMO(α) → LUMO+1(α) (37%), respectively, transitions and may be considered as a combination of π(L) → π*(L)/dπ*(Mn) transitions.

Hirshfeld surface analysis:

Hirshfeld surface analysis was performed to investigate supramolecular interactions in **1**. Complex **1** is mapped over d_{norm} (range of –0.1 to 1.5 Å), shape index (range of –1.0–1.0 Å) and curved (range of –4.0–0.4) respectively and presented in Figs. 13 and 14, respectively. To visualize the different supramolecular interactions surfaces are kept transparent during mapping. Hydrogen bonding interactions between the nitrogen atom of azide and hydrogen atoms of the

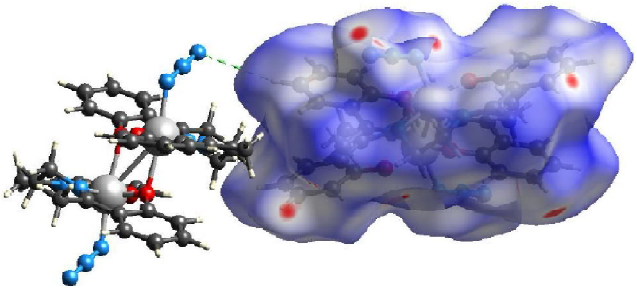

Fig. 13. Surface mapping of complex **1** over d_{norm}.

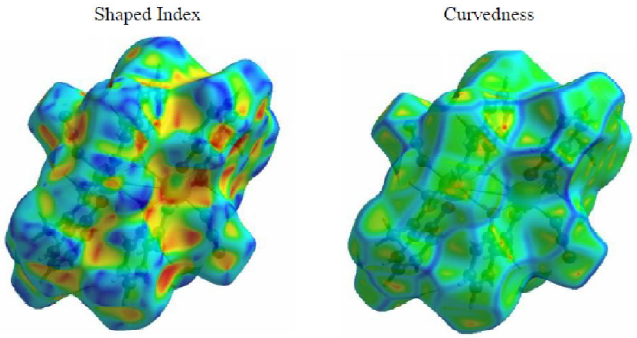

Fig. 14. Surface mapping of complex **1** over shaped index and curvedness.

phenyl ring has been found to be predominant as bright red area in the Hirshfeld surfaces in complex **1**. Light color in the surfaces represents the other longer and weaker interactions present in **1**. All type of intermolecular interactions is present in fingerprint plots. So, fingerprint plots should be decomposed to have idea of individual contacts. Complementary regions are obtained in the decomposed fingerprint plot where one molecule acts as a donor ($d_e > d_i$) (bottom left of fingerprint plot) and the other as an acceptor ($d_e < d_i$) (bottom right of fingerprint plot). N···H/H···N, O···H/H···O and H···H interactions comprise 28.00%, 4.30% and 49.60% of the total Hirshfeld surface in complex **1**. N···H interactions are assigned around 14.7% of the total Hirshfeld surface and represented by a spike (d_i = 1.05 Å, d_e = 1.4 Å) in the bottom left (donor) area. Whereas H···N interactions are represented by a spike (d_i = 1.40 Å, d_e = 1.08 Å) in the bottom right (acceptor) region and assigned around 13.3% of the total Hirshfeld surface (Fig. 15). The O···H/H···O contacts are negligible in comparison.

Conclusion

The competence of the newly synthesized azido adduct of Schiff base manganese(III) phenoxo-bridged dimer complex towards sensing of benzene is a new prospect of this class of compounds. The synthesis of the compound has been illustrated together with its relevant characterization. Absorption spectral method has been implemented for the sensing of the benzene. Interaction of the aromatic moiety of the complex **1** with the aromatic hydrocarbon analyte was strongly suspected and was found to have agreeable matches with the corresponding IR spectra. Besides, complex **1** showed nice catalytic activity towards 2-aminophenol oxidation. A functional model for phenoxazinone synthase like ac-

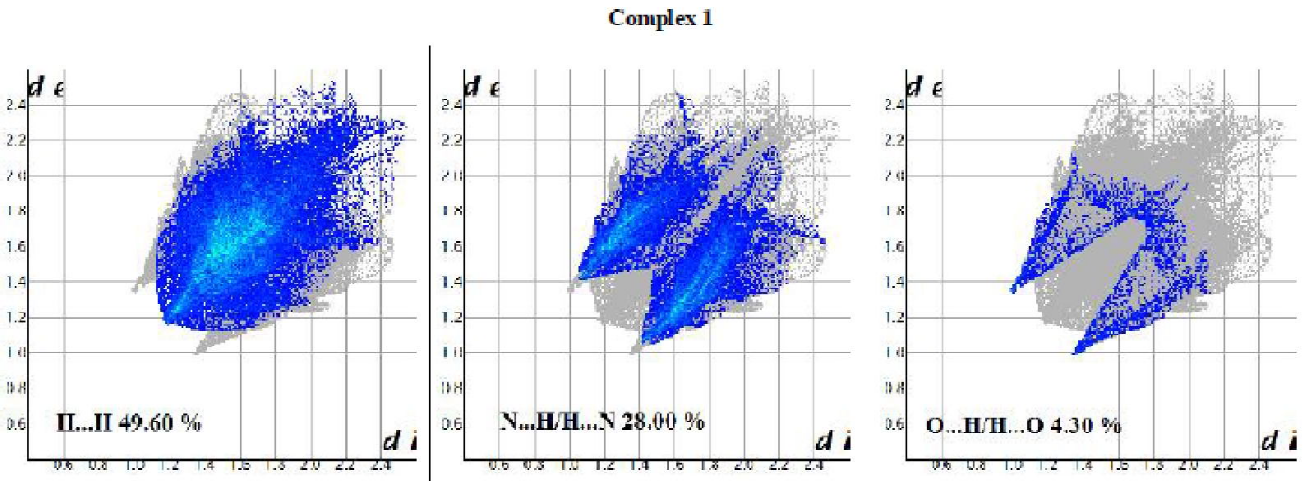

Fig. 15. Decomposed fingerprint plot of complex **1**.

tivity has been established using Michaelis-Menten model. Michaelis binding constant (K_M), V_{max} and turnover number (K_{cat}) were calculated to be (1.09±0.3)×10^{-2} *M*, 5.77×10^{-8} *M* s^{-1} and 20.77 h^{-1}, respectively. Furthermore, the structural and electronic parameters of complex **1** have been justified by DFT and TD-DFT computation. Also Hirshfeld fingerprint plotting has been performed to visualize the close contacts like hydrogen bonding.

Acknowledgements

Financial support from DST [Sanction no. SR/FT/CS-060/2009] and UGC [Sanction no. F.38-5/2009 (SR)], New Delhi to SS are gratefully acknowledged. KS acknowledges UGC CAS-V for funding.

References

1. E. J. Larson, V. L. Pecoraro and V. L. Pecoraro (Ed), "Manganese Redox Enzymes", VCH Publishers, New York, 1992, p. 1.
2. A. Escuer, J. Esteban, S. P. Perlepes and T. C. Stamatatos, *Coord. Chem. Rev.,* 2014, **275**, 87.
3. R. Gupta, T. Taguchi, B. L. Kaiser, E. L. Bominaar, J. Yano, M. P. Hendrich and A. S. Borovik, *Proc. Nat. Acad. Sci.*, 2015, **112**, 5319.
4. J. Limburg, J. S. Vrettos, L. M. Liable-Sands, A. L. Rheingold, R. H. Crabtree and G. W. Brudvig, *Science*, 1999, **283**, 1524.
5. L. Sun, M. K. Raymond, A. Magnuson, D. L. Gourrie'rec, M. Tamm, M. Abrahamsson, P. H. Kenéz, J. Mårtensson, G. Stenhagen, L. Hammarstrom, S. Styring and B. A. Kermark, *J. Inorg. Biochem.*, 2000, **78**, 15.
6. H. H. Ko, J. H. Lim, H. C. Kim and C. S. Hong, *Inorg. Chem.*, 2006, **45**, 8847.
7. S. Nastase, F. Tuna, C. Maxim, C. A. Muryn, N. Avarvari, R. E. Winpenny and M. Andruh, *Cryst. Growth Des.*, 2007, **7**, 1825.
8. Z. Lu, M. Yuan, F. Pan, S. Gao, D. Zhang and D. Zhu, *Inorg. Chem.*, 2006, **45**, 3538.
9. S. Saha, D. Mal, S. Koner, A. Bhattacherjee, P. Gutlich, S. Mondal, M. Mukherjee and K.-I. Okamoto, *Polyhedron*, 2004, **23**, 1811.
10. A. Panja, N. Shaikh, P. Vojtisek, S. Gao and P. Banerjee, *New J. Chem.*, 2002, **26**, 1025.
11. M. Yuan, F. Zhao, W. Zhang, Z.-M. Wang and S. Gao, *Inorg. Chem.*, 2007, **46**, 11235.
12. H. Li, Z. J. Zhong, C. Y. Duan, X. Z. You, T. C. W. Mak and B. Wu, *Inorg. Chim. Acta*, 1998, **271**, 99.
13. P. Bhowmik, H. P. Nayek, M. Corbella, N. Aliaga-Alcalde and S. Chattopadhyay, *Dalton Trans.*, 2011, **40**, 7916.
14. M. A. Carpenter, S. Mathur and A. Kolmakov, "Metal Oxide Nanomaterials for Chemical Sensors", 1st ed., Springer, New York, 2013.
15. J. H. Yoon, H. C. Kim, W. R. Lee, D. W. Ryu, J. W. Lee, S. W. Yoon, B. J. Suh and C. S. Hong, *Inorg Chem.*, 2011, **50**, 10777.
16. T.-H. Tran-Thi, R. Dagnelie, S. Crunaire and L. Nicole, *Chem. Soc. Rev.*, 2011, **40**, 621.
17. P. K. Sekhar and K. Subramaniyam, *Lett.*, 2014, **3**, B1.
18. H.-J. Kim, J.-W. Yoon, K.-I. Choi, H. W. Jang, A. Umar and J.-H. Lee, *Nanoscale*, 2013, **5**, 7066.
19. S. Chatterjee, M. Castro and J. F. Feller, *J. Mater. Chem.*, 2013, **36**, 4563.
20. J. Hodgkinson and R. P. Tatam, *Meas. Sci. Technol.*, 2013, **24**, 012004.
21. J. M. Bingham, J. N. Anker, L. E. Kreno and R. P. V. Duyne, *J. Am. Chem. Soc.*, 2010, **132**, 17358.
22. L. Brigo, N. Michieli, L. Artiglia, C. Scian, G. A. Rizzi, G. Granozzi, G. Mattei, A. Martucci and G. Brusatin, *Appl. Mater. Interfaces*, 2014, **6**, 7773.
23. F. Faridbod, M. R. Ganjali, R. Dinarvand, P. Norouzi and S. Riahli, *Sensors*, 2008, **8**, 1645.
24. P. P. Chakrabarty, S. Saha, K. Sen, A. D. Jana, D. Dey, D. Schollmeyer and S. García-Granda, *RSC Adv.*, 2014, **4**, 40794.
25. P. P. Chakrabarty, S. Giri, K. Sen, S. Saha, A. D. Jana, S. García-Granda, S. Haldar and M. Bera, *J. Coord. Chem.*, 2016, **69**, 2881.
26. M. Garai, D. Dey, R. H. Yadav, M. Maji, R. A. Chowdhury and B. Biswas, *J. Chem. Sci.*, 2017, **129**, 1520.
27. A. Panja, *Dalton Trans.*, 2014, **43**, 7760.
28. M. Garai, D. Dey, R. H. Yadav, R. A. Chowdhury, M. Maji and B. Biswas, *ChemistrySelect*, 2017, **2**, 11047.
29. B. Biswas and P. P. Sengupta, *J. Indian Chem. Soc.*, 2017, **94**, 578.
30. C. Mukherjee, T. Weyhermüller, E. Bothe, E. Rentschler and P. A. Chaudhuri, *Inorg. Chem.*, 2007, **46**, 9895.
31. M. B. Banerjee, S. Pradhan, R. B. Roy, B. Tudu, D. K. Das, R. Bandyopadhyay and P. Pramanik, *IEEE Sensors Journal,* 2018, **1**.
32. G. C. Gil, R. J. Mitchell, S. T. Chang and M. B. Gu, *Biosens. Bioelectron.*, 2000, **15**, 23.
33. T. Xu, P. Xu, D. Zheng, H. Yu and X. Li, *Anal. Chem.*, 2016, **24**, 12234.
34. K. A. McGee, B. J. Marquardt and K. R. Mann, *Inorg. Chem.*, 2008, **47**, 9143.
35. Y. Gurbuz, W. P. Kang, J. L. Davidson and D. V. Kerns, *Sens. Actuators B,* 2004, **99**, 207.
36. R. Kadir, A. Yimit, H. Ablat, M. Mahmut and K. Itoh, *Environ. Sci. Technol.*, 2009, **43**, 5113.
37. W. Sha, S. Ni and C. Zheng, *Sens. Actuators B*, 2015, **209**, 297.
38. M. T. Ke, M. T. Lee, C. Y. Lee and L. M. Fu, *Sensors*, 2009, **9**, 2895.

39. D. Ionov, G. Yurasik, Y. Kononevich, V. Sazhnikov, A. Muzafarov and M. Alfimov, *Procedia Eng.*, 2016, **168**, 341.
40. M. J. Frisch, G. W. Trucks, H. B. Schlegel, G. E. Scuseria, M. A. Robb, J. R. Cheeseman, G. Scalmani, V. Barone, B. Mennucci, G. A. Petersson, H. Nakatsuji, M. Caricato, X. Li, H. P. Hratchian, A. F. Izmaylov, J. Bloino, G. Zheng, J. L. Sonnenberg, M. Hada, M. Ehara, K. Toyota, R. Fukuda, J. Hasegawa, M. Ishida, T. Nakajima, Y. Honda, O. Kitao, H. Nakai, T. Vreven, J. A. Montgomery (Jr.), J. E. Peralta, F. Ogliaro, M. Bearpark, J. J. Heyd, E. Brothers, K. N. Kudin, V. N. Staroverov, R. Kobayashi, J. Normand, K. Raghavachari, A. Rendell, J. C. Burant, S. S. Iyengar, J. Tomasi, M. Cossi, N. Rega, J. M. Millam, M. Klene, J. E. Knox, J. B. Cross, V. Bakken, C. Adamo, J. Jaramillo, R. Gomperts, R. E. Stratmann, O. Yazyev, A. J. Austin, R. Cammi, C. Pomelli, J. W. Ochterski, R. L. Martin, K. Morokuma, V. G. Zakrzewski, G. A. Voth, P. Salvador, J. J. Dannenberg, S. Dapprich, A. D. Daniels, Ö. Farkas, J. B. Foresman, J. V. Ortiz and J. Cioslowski Fox D J GAUSSIAN **09** Revision D.01 Gaussian Inc., Wallingford CT, 2009.
41. A. D. Becke, *J. Chem. Phys.*, 1993, **98**, 5648.
42. C. Lee, W. Yang and R. G. Parr, *Phys. Rev. B*, 1988, **37**, 785.
43. P. J. Hay and W. R. Wadt, *J. Chem. Phys.*, 1985, **82**, 270.
44. W. R. Wadt and P. J. Hay, *J. Chem. Phys.*, 1985, **82**, 284.
45. P. J. Hay and W. R. Wadt, *J. Chem. Phys.*, 1985, **82**, 299.
46. G. A. Petersson, A. Bennett, T. G. Tensfeldt, M. A. Al-Laham, W. A. Shirley and J. A. Mantzaris, *J. Chem. Phys.*, 1988, **89**, 2193.
47. G. A. Petersson and M. A. Al-Laham, *J. Chem. Phys.*, 1991, **94**, 6081.
48. R. Bauernschmitt and R. Ahlrichs, *Chem. Phys. Lett.*, 1996, **256**, 454.
49. R. E. Stratmann, G. E. Scuseria and M. J. Frisch, *J. Chem. Phys.*, 1998, **109**, 8218.
50. M. E. Casida, C. Jamorski, K. C. Casida and D. R. Salahub, *J. Chem. Phys.*, 1998, **108**, 4439.
51. V. Barone and M. Cossi, *J. Phys. Chem. A*, 1998, **102**, 1995.
52. M. Cossi and V. Barone, *J. Chem. Phys.*, 2001, **115**, 4708.
53. M. Cossi, N. Rega, G. Scalmani and V. Barone, *J. Comput. Chem.*, 2003, **24**, 669.
54. N. M. O'Boyle, A. L. Tenderholt and K. M. A. Langner, *J. Comput. Chem.*, 2008, **29**, 839.
55. S. K. Wolff, D. J. Grimwood, D. J. McKinnon, D. Jayatilaka and M. A Spackman, Crystal Explorer 3.1, University of Western Australia, Perth, Australia, 2007.
56. J. J. McKinnon, D. Jayatilaka and M. A. Spackman, *Chem. Commun.*, 2007, 3814.
57. S. Kendric, "The Science of Photobiology", ed. Kendric C. Smith, Plenum Publishing Corporation, New York, 1977.